Journal of Applied Polymer Science

# Enhanced mechanical and electrical properties of nylon-6 composite by using carbon fiber/graphene multiscale structure as additive

**Chong-Guang Zang, Xiang-Dong Zhu, Qing-Jie Jiao**
State Key Laboratory of Explosive Science and Technology, Beijing Institute of Technology, Beijing 100081, People's Republic of China
Correspondence to: C. G. Zang (E-mail: zangchongguang@bit.edu.cn)

**ABSTRACT:** In order to improve the mechanical properties and electrical conductivity of nylon-6 (PA6) composites, a highly effective multiscale structure filler comprising poly(diallyldimethylammonium chloride) (PDDA)-modified graphene and negatively surface-charged carbon fiber was synthesized in this study. For this, the graphene used a top-down method for synthesis by exfoliating graphite oxide (GO) through focused solar radiation on it and then modified its surface by using a polyelectrolyte. The carbon fiber (CF) surface was functionalized by an acid oxidation method. The multiscale structure was manufactured via the electrostatic interaction between the positively charged solar graphene (SG) and oppositely charged CF by homogeneous mixing. Scanning electron microscopy (SEM) images of the fracture surface of the PA6 composites exhibited that the carbon fiber/graphene multiscale structure possessed better dispersion and compatibility than those of individual CF and SG did. Thus, the impact strength, bending properties, and electrical conductivity of the PA6 composites were enhanced. © 2015 Wiley Periodicals, Inc. J. Appl. Polym. Sci. **2015**, *132*, 41968.

**KEYWORDS:** fibers; graphene and fullerenes; mechanical properties; nanotubes; polyamides

Received 10 August 2014; accepted 11 January 2015
**DOI: 10.1002/app.41968**

## INTRODUCTION

It is well known that polymer/filler composites with their favorable performances have attracted tremendous attention.[1–4] Polymer composites with carbon-based fillers can improve mechanical properties, thermal and electrical conductivities have many potential applications that include thermal management, electronics, fuel cells, and transportation.[5] Carbon-based fillers, such as carbon nanotubes (CNTs), carbon fiber (CF), and graphene (G),[6–16] can improve mechanical properties and the thermal and electrical conductivities of polymer composites. Among different types of carbon-based fillers, the high electrical conductivity, better transfer channels, and high accessible surface area of graphene make it potential in improving the performances of composites materials.[12,13,15–18]

However, to a large extent, the performance of graphene/polymer composites, controlled by dispersion and compatibility of graphene in polymeric matrices. Due to the large Van der Waals forces and strong $\pi$–$\pi$ interactions, the large surface between graphene nanosheets tends to aggregation and stacking in polymer matrix.[19–21] In order to solve the problem, scientists had developed some useful methods with respect to improve the dispersibility of graphene in polymer matrix. A common method is acid oxidations that can improve the dispersion and compatibility of graphene-based materials in polymer. Nevertheless, the acid oxidation may generate structure damage of graphitic structure, resulting in the loss of nature properties of graphene-based materials.[22,23] Using a hybrid filler system that contains graphene was another way to improve the dispersion of graphene, such as graphene/carbon nanotubes, available but with high cost.[5]

Recently, a new concept of multiscale filler containing fibers together with graphene on the surface of fibers was used to improve the performance of polymer composites.[24,25] In Ref. 24, graphene oxide (GO) was coated onto the surface of carbon fiber, which can significantly enhance the interfacial and mechanical properties with very low percent of GO. In Ref. 25, the author assembled GO and glass fiber via electrostatic self-assembling of the oppositely charged GO and amino coupling agent-modified fiber largely enhance the crystallization polymer composites. However, GO is insulating as its conductivity is $\sim 10^{-5}$ $Sm^{-1}$,[26] so the conductivity of polymer composites was not considered in these papers. Thus, directly coat the graphene onto the surface of fibers will be an effective method in preserving graphene physical and electronic properties and improving graphene dispersion within the polymer matrix for enhancing the performance of polymer composites.

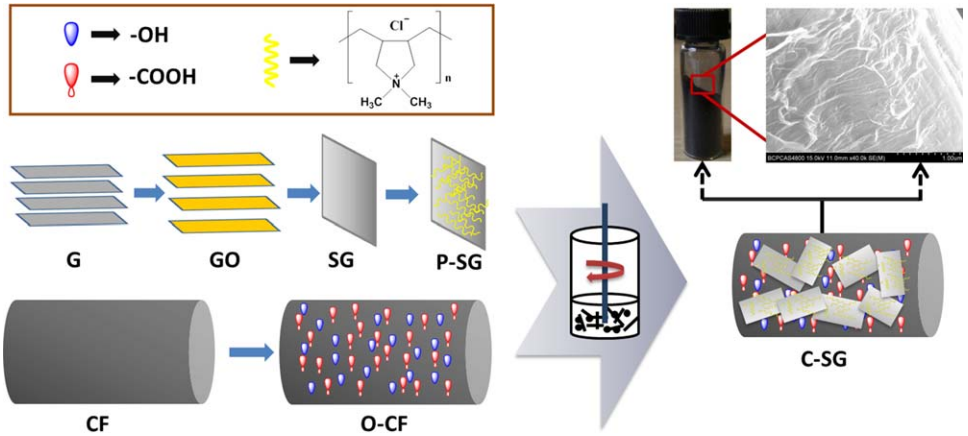


**Figure 1.** or the process of synthesizing the carbon fiber/graphene multiscale structure. [Color figure can be viewed in the online issue, which is available at wileyonlinelibrary.com.]

To the best of our knowledge, it had not been reported in the literature.

Therefore, in this study, we designed an alternative strategy for the fabrication of multiscale filler with graphene and carbon fiber to improve the mechanical properties and electrical conductivity of PA6 composite. By the surface modification, the graphene could be coated on the CF surface via the electrostatic interaction. This route absorbs the advantage of predecessor's techniques for the dispersion of graphene in resin. Consequently, the carbon fiber/graphene multiscale fillers system exhibits a remarkable enhancement of mechanical properties and electrical conductivity of PA6 composites which were demonstrated by compared with the individual graphene and carbon fiber.

## EXPERIMENTAL

### Materials

Natural graphite flakes with an average diameter of 10 $\mu$m were purchased from Qingdao Hensen Graphite (China). CF was produced by Liaoning Anke Carbon Fibre Co., and used model of 12KF with a resistivity of 1.6 Ωcm, diameter of 6.5 $\mu$m, and length of 1 mm. Poly-(diallyldimethyl ammonium chloride) (PDDA, 20 wt % in water, $M_W = 20{,}000 - 350{,}000$, Aldrich) were used as received. Sodium nitrate ($NaNO_3$, 99.5%) and potassium permanganate ($KMnO_4$, 99.5%) were obtained from Beijing Chemical Works. Concentrated sulfuric acid ($H_2SO_4$, 98%), and concentrated nitric acid ($HNO_3$, 98%) were purchased from Sinopharm Chemical Reagent Beijing Co., Ltd. Sodium chloride (NaCl, Aldrich), Ultrapure water (>18 MΩcm) was used throughout the experiment.

### Experimental Procedure

**Preparation of Graphene.** GO was prepared by using a modified Hummers and Offeman's method.[27,28] The fabrication of graphene employed the method of solar exfoliation of GO.[26] For this, about 100 mg GO powder was placed in a glass petri dish and focus the solar radiation on it by a convex lens. The focused solar radiation with high intensity directed toward GO imparts sufficient energy needed for exfoliation within few seconds. Due to the focused solar radiation interacts with the GO powder, the color of it changed from light brown to dark black accompanied by a fast volume expansion, indicating the reduction of GO to graphene finished. The sample was named as "SG" for solar graphene.

**Preparation of PDDA-Modified Graphene.** SG was modified with PDDA by the following method.[29] About 200 mg SG was initially ultrasonic (Frequency: 40 KHz, Model: KQ5200E, Kun Shan Ultrasonic Instruments Co., Ltd) dispersed in 800 mL ultrapure water for 30 min with a 0.5 wt % concentration of PDDA, which played a role of the functionalizing polyelectrolyte and caused the graphene stable dispersion in the water, and then, the NaCl was slowly added into the solution until the concentration reach to 0.5 wt %. Due to the presence of NaCl, the configuration of the polymeric chain was tremendously varied in polyelectrolyte which strengthened the functionalization. Finally, the PDDA-modified graphene was filtered and cleaned with ultrapure water to get rid of the redundant PDDA, and the obtained solid was put into a vacuum oven for 24 h at 70°C.The PDDA-functionalized graphene was named "P-SG."

**Introduction of Graphene on the Carbon Fiber.** In order to introduce the P-SG onto the surface of CF, the following works should be adopted:

1. In order to reduce the effect of commercial layer on the surface of raw CF, the raw CF was refluxed by acetone for 48 h before used.
2. In order to introduce oxygen-containing groups (negative charge) on the surface of CF, CF was ultrasonic treated with 69% $HNO_3$ at 60°C by reflux for 4 h. The resulting oxidized CF was named" O-CF."

The multiscale structure of carbon fiber and graphene were obtained by mixing the suspension of O-CF and P-SG. The P-SG was immersed in ultrapure water and then ultrasonicated for 1 h, followed that the O-CF in the ratio 100: 1 (O-CF: P-SG) was added into the suspension and then stirred for 12 h. Then, the solution was filtered, and the final product was dried in a vacuum oven at 50°C. The final sample was

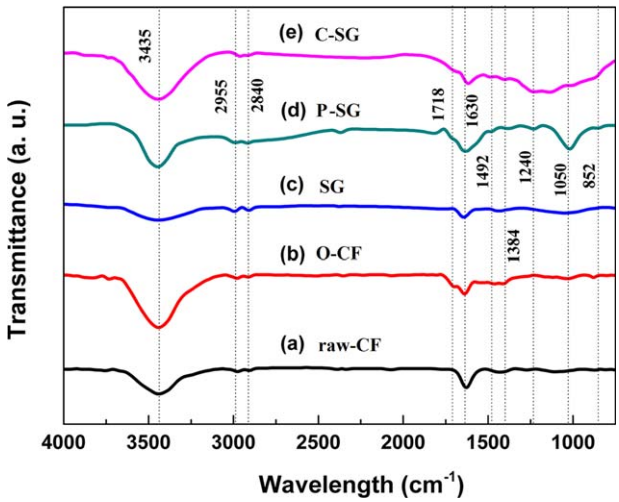


**Figure 2.** FTIR spectra of (a) raw carbon fiber, (b) acid oxide carbon fiber, (c) solar graphene, (d) PDDA-functionalized graphene, and (e) carbon fiber/graphene composite. [Color figure can be viewed in the online issue, which is available at wileyonlinelibrary.com.]

named as "C-SG." The overall synthetic pathway is shown in Figure 1.

### Preparation of Composites

The PA6 composites were manufactured by melt compounding at 250°C through a twin-screw mixer. Compounding was performed with a screw speed of 100 rpm/min for 10 min. The obtained different kinds of PA6 composites particles were compression under a pressure of 150 bar for 10 min at 250°C and then cool the mold to room temperature for obtaining different kinds of specimens which would be used for electrical and mechanical tests.

### Characterization and Instruments

A Fourier transform infrared (FTIR) spectrometer was used for detecting the functional groups in the range of 750–4000 $cm^{-1}$ by using KBr pellet method. A Netzsch TG 209F1 thermogravimetric was employed for the thermogravimetric analysis (TGA) under a nitrogen atmosphere at a heating rate of 20°C from ambient temperature to 800°C. The X-ray diffraction (XRD) measurements analyzed via a Bruker D8 X-ray diffractometer with nickel filtered Cu-K$\alpha$ as the X-ray source. The 2$\theta$ range of 10°–75° with a step size of 0.014° was recorded. The morphological observations were executed using a cold field emission scanning electron microscopy (SEM; S4800, Hitachi High-Technologies Corp.). Transmission electron microscopy (TEM) image was taken on a JEOL JEM-2100 to characterize the microstructure of SG. The Charpy impact tests were performed on the procedure of ISO by an impact tester (Charby XCL-50), and the specimen dimensions were 64 × 10 × 4 $mm^3$. The bending properties of PA6 composites were measured on the basis of and ASTM procedure by an electromechanical universal testing machine (CMT4104) at room temperature with the specimens dimensions of 70 × 12.7 ×3 $mm^3$. An EST 991 electric and electrostatic shielding materials volume resistivity measure instrument was used for measuring the direct-current (dc) bulk electrical resistivity (Ωcm) of the prepared specimens through a four-contact scheme method with the dimensions of 20 × 10 × 2 $mm^3$ at steady state and room temperature.

## RESULTS AND DISCUSSION

### FTIR Analysis

The functional groups on the surface of the CF and graphene were verified by FTIR spectroscopic measurements. Figure 2 shows the FTIR spectrum for (a) raw-CF, (b) O-CF, (c) SG, (d) P-SG, and (e) C-SG. All the samples show a very strong and broad band between 3200 and 3600 $cm^{-1}$ is due to the stretching mode of the O—H bond.[30] The bands in all of the samples around 2955 and 2840 $cm^{-1}$ were attributed to the asymmetric ($aCH_2$) and symmetric ($sCH_2$) stretching mode of the C—H bond and the band at 1630 $cm^{-1}$ corresponds to the C=C band.[31,32] The FTIR curves of raw-CF and SG show a relative smooth trend except the absorption band around 3435 $cm^{-1}$ and 1630 $cm^{-1}$ were due to the stretching mode of O—H and C=C, respectively. After treating with $HNO_3$, the O-CF exhibits the following characteristic features: C=O stretching of —COOH at 1718 $cm^{-1}$, C—O stretching of C—OH at 1050 $cm^{-1}$, O—H vibrations of C—OH groups around at

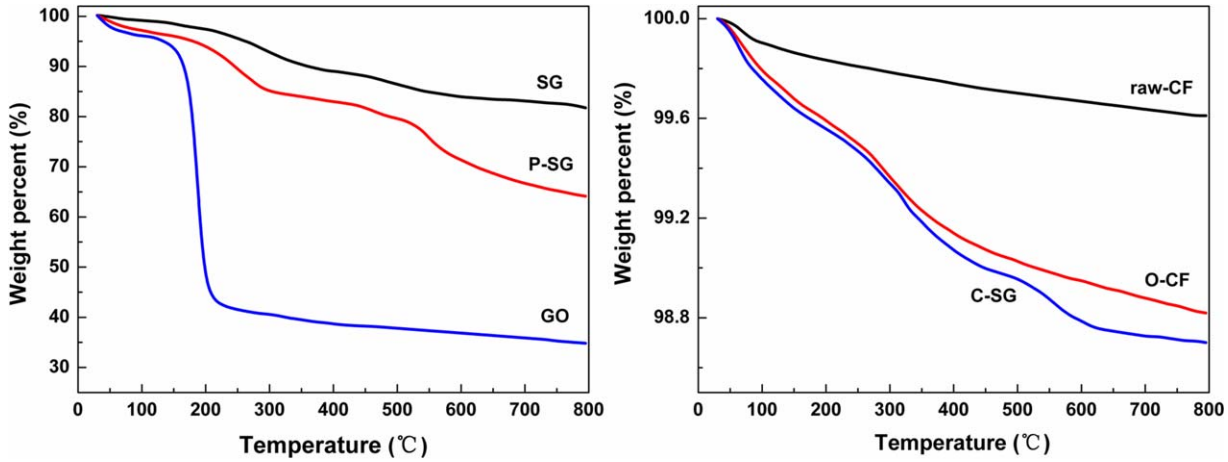


**Figure 3.** TGA curves of different types of graphene and carbon fiber. [Color figure can be viewed in the online issue, which is available at wileyonlinelibrary.com.]

1384 $cm^{-1}$. All of the features confirmed that surface of the O-CF was grafted with oxygen containing functional groups, such as —COOH, —OH, etc, successfully. The solar reduction of GO to SG was certified by the dramatic decrease in peak intensity of the oxygen functional groups in the FTIR spectrum. The appearance of new peaks at around 852 and 1492 $cm^{-1}$ can be attributable to the C—N band in the adsorbed PDDA on the P-SG,[33] which proved the successful adsorption of PDDA onto the SG. To some extent, the FTIR of C-SG exhibits the combination of the absorption peak by assembling O-CF with P-SG, confirmed that SG was adsorbed onto the surface of O-CF successfully.

### TGA Analysis

TGA is a powerful tool to investigate the thermal stability of carbon-based materials because of different forms of carbon exhibit different oxidation behaviors.[34] Figure 3 shows the TGA curves recorded under nitrogen for GO, SG, P-SG, raw-CF, O-CF, and C-SG. As can be seen, GO exhibits a relatively poor thermal stability with a rather low onset temperature (150–250°C) for decomposition of the most of the labile oxygen groups on GO. The weight loss below 150°C is due to the removal of adsorbed water and decomposition of some oxygen-containing functional groups. After exfoliation of GO with focused solar radiation, the thermal stability of SG enhanced dramatically indicates a successful reduction process. The TGA spectra of P-SG with 9% weight loss of the decomposition of PDDA from 280 to 600°C,[35,36] means that the PDDA had adsorbed on the surface of SG successfully. The raw-CF exhibits an excellent thermal stability with a weight loss of 0.5% was aroused by amorphous carbon, moisture, metal particles, and volatile carbonaceous impurities. By the oxidization of nitric acid with raw-CF, the O-CF shows the decomposition of oxygen-containing functional groups (—COOH, —OH, etc.) at the temperature of 180–300°C. The C-SG exhibits a similar tendency of TGA curve compared with O-CF. Although the content of SG less than 1 wt % in the multiscale structure, the C-SG shows about 0.2% weight loss of PDDA up to around 600°C.

### XRD Analysis

Figure 4 shows the powder X-ray diffraction pattern of (a) graphite, (b) GO, (c) SG, (d) CF, and (e) C-SG. The peak at 26.3° corresponds to the characteristic peak of the C (002) plane in graphite with a *d*-spacing of 0.339 nm. The peak of C (002) in GO shifts to 11.6° corresponding to an inter layer *d*-spacing of 0.762 nm, which is aroused by the oxygen-containing functional groups which insert into the graphite sheets. Owing to the rapid heating of GO with the focused solar radiation, the XRD curve of SG shows a broaden peak of C (002) ranging from 15° to 31° (Figure 4c). The disappearance of 10.9° peak indicates that the oxygen-containing functional groups had been decomposed and escaped from the graphite layers. The broadening band either due to the small size of the layers or a relatively short domain order of stacked sheets.[25] Figure 4d shows the XRD of raw-CF exhibits a broadened feature from 18° to 28°. The width in XRD pattern can be attributed to turbostratic structure of graphite in carbon fiber, which is similar to the structure of graphene. As discussed previously, the carbon fiber belongs to one of the form of graphite and hence exhibits

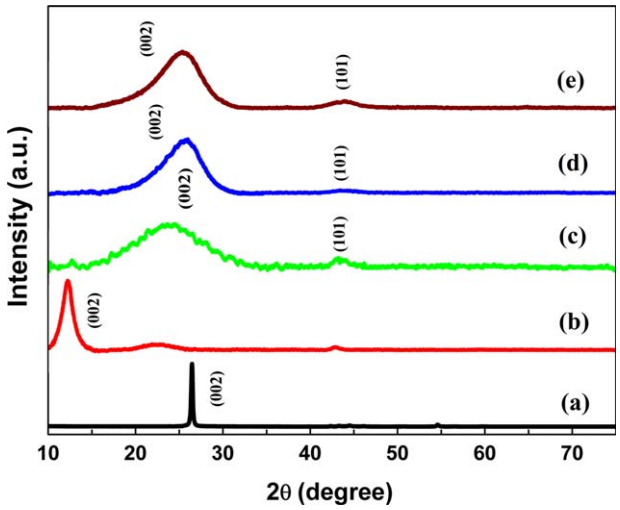


**Figure 4.** X-ray diffractograms of (a) graphite, (b) graphite oxide, (c) solar graphene, (d) carbon fiber, and (e) carbon fiber/graphene multiscale structure. [Color figure can be viewed in the online issue, which is available at wileyonlinelibrary.com.]

almost the same *d*-spacing with graphite. For C-SG, the XRD pattern has a similar tendency with the raw-CF, due to the content of SG is less than 1 wt % on the surface of CF. However, by careful examination, the multiscale structure shows a wider feature of C (002) from 16.5° to 30°. This may be ascribed that the ultrathin SG sheets on the curved surface of the CF lead to the increase the width of XRD pattern.

### Morphological Analysis

Figure 5 shows the morphology of different kinds of carbon fiber and graphene. It can be seen from Figure 5a that the surface of the raw-CF is very pure and smooth due to the epoxy sizing agent layer. The SEM image in Figure 5b shows the CF appears some ravines on its surface which suggest that the process of oxidation was effective. The micrographs in Figures 5(c,d) show the wrinkle in the exfoliated graphene sheets. Because the thickness of graphene is very small, the graphene possesses a large aspect ratio, which is an important factor in enhancing contact area with polymer matrix.[2] In multiscale structure [Figure 5(e,f)], it is evident that the graphene was successfully covered on the surface of CF. It can be seen that most of the graphene was contacted closely with the surface of the CF as shown in Figure 5f. Through comparing the Figure 5a with Figure 5e, it can be seen the diameter of C-SG is larger than raw-CF, changed from 6.56 $\mu$m to 7.03 $\mu$m. Moreover, due to the Van der Waal forces, some of graphene was aggregated and formed bundles, some like the clouds float on the CF, resulting in the surface of CF become circuitous, which may be useful for improving the contact area between filler and polymer. The complicated morphology and larger diameter of CF is beneficial to enhance the composites properties, which will discussed in detail in the following sections.

The morphology of the fractured surfaces of PA6 composites were investigated by SEM. To some extent, the fractured surfaces could display the dispersion and compatibility of fillers in polymer matrix, as shown in Figure 6. Figures 6(a,b) show

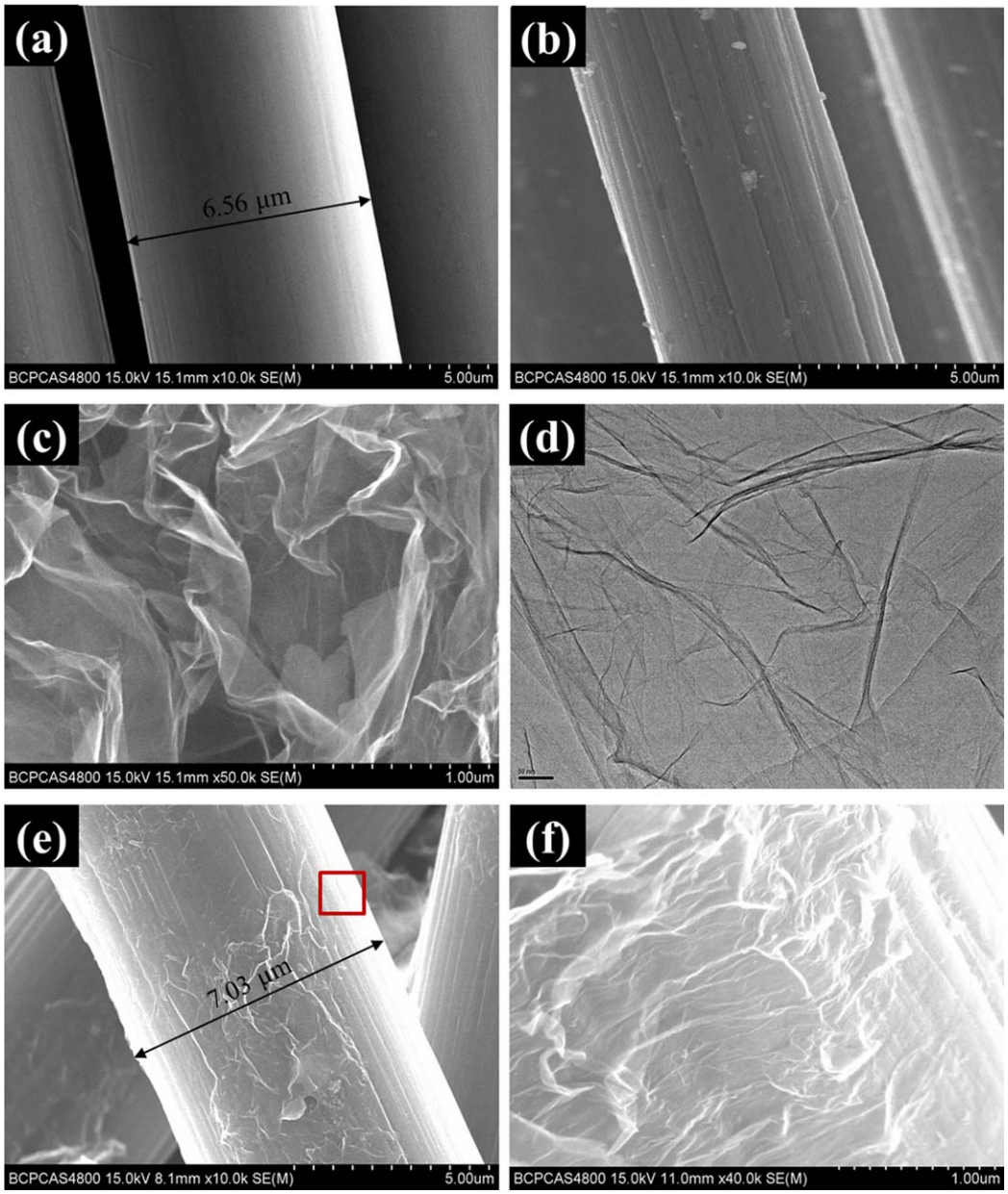


**Figure 5.** SEM images of (a) raw carbon fiber, (b) acid oxide carbon fiber, (c) solar graphene, (e) carbon fiber/graphene multiscale structure, and (f) the square area in image (e) with higher magnicfication and TEM image of (d) solar graphene. [Color figure can be viewed in the online issue, which is available at wileyonlinelibrary.com.]

exhibits the poor compatibility and low adhesion between fillers and polymer matrix of the raw-CF/PA6 composite, which will further influence the improvement in the mechanical and electrical properties of the polymer composites. Furthermore, most of the raw-CF scattered in PA6 matrix placed with a same orientation, resulting in the formation of electrically conductive path needs for more fillers. The SEM images of the PA6 composites containing SG shows poor dispersion due to the aggregated SG, as the red circle shown in Figure 6(c,d), Figure 7 shows the element difference between the aggregation of SG and the PA6 resin. In the SG aggregation, all of the elements were carbon, while the other region contains oxygen element. Moreover, the SG aggregation could sterically hinder polymer flow, resulting in formation of defects,[2] easy to form the location of stress concentration. As shown in Figure 6(e,f), the composite-containing C-SG shows a better dispersion and homogeneity of C-SG in PA6 matrix. Attribute to the electronegativity group of —COOH in PA6, the PDDA could enhance the compatibility between graphene and PA6 matrix, and hence, the graphene on the surface of carbon fiber just likes a double-faced adhesive tape, links the carbon fiber with PA6 matrix. Moreover, it can be seen that the C-SG are surrounded tightly by the PA6 matrix, which means that the enhanced adhesion between fillers and polymer matrix. Interestingly, the C-SG scattered at a higher degree in three-dimensional (3D) than the raw-CF in matrix, which have positive influences on

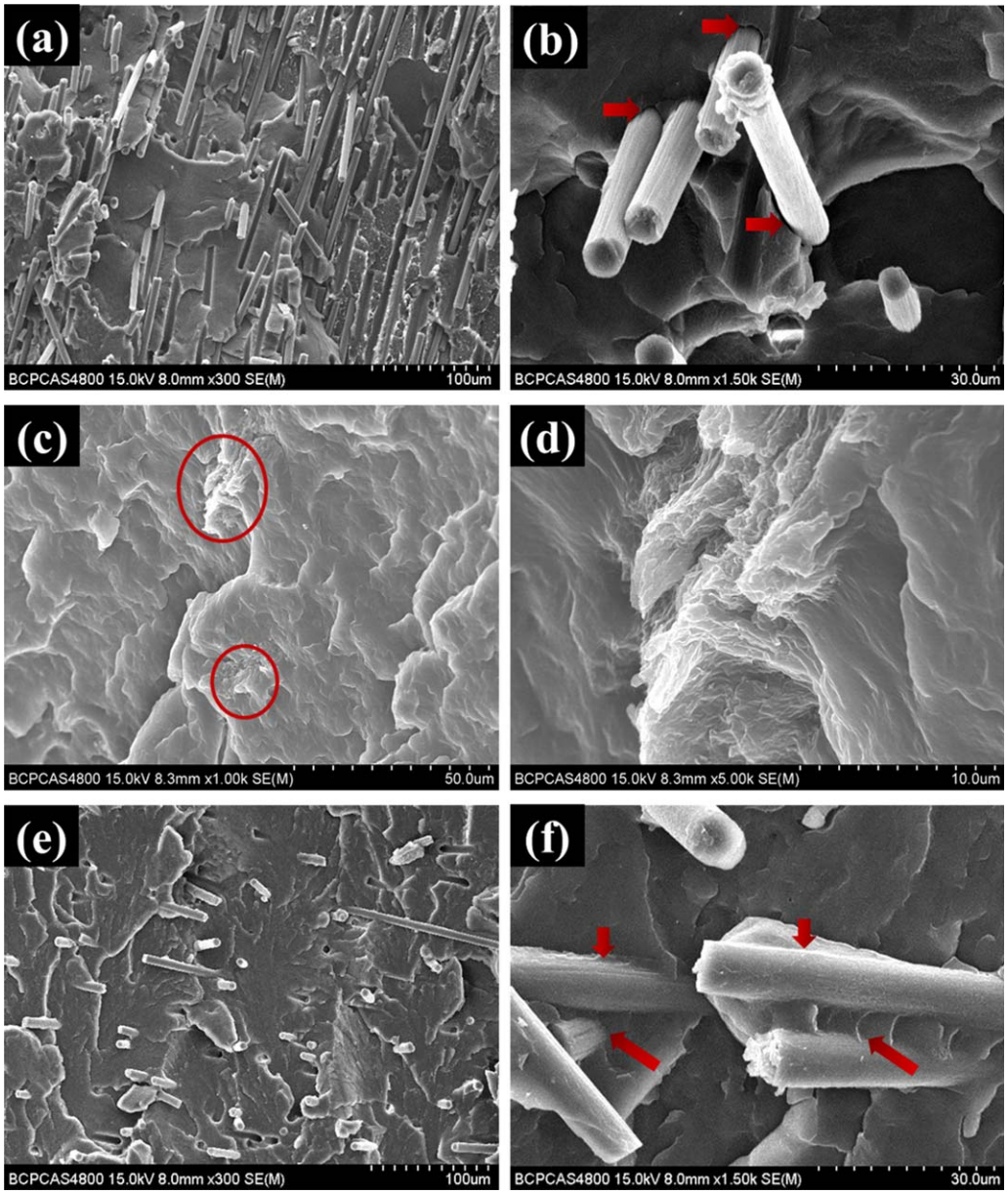


**Figure 6.** SEM images of (a) and (b) raw-CF/PA6 composite, (c) and (d) SG/PA6 composite, (e) and (f) C-SG/PA6 composite at lower and higher magnifications. [Color figure can be viewed in the online issue, which is available at wileyonlinelibrary.com.]

mechanical properties and electrical conductivity of the polymer composites.

### Mechanical Properties

Figure 8 shows the results of impact property tests for pure PA6 and PA6 composites. Obviously, the SG/PA6 composite exhibits dropped impact strength with increase in the content of SG, due to the aggregation of SG sheets in the matrix. The agglomerates of SG behave like micrometer-sized fillers with relatively low surface area with polymer and form holes and voids between SG and PA6, resulting in the poor elasticity of SG/PA6 composites. The impact strength of raw-CF/PA6 composites shows a significant increase compared to the pure PA6 resin. It was found that when the content of raw-CF is about 11 wt %, the impact strength of raw-CF/PA6 composite reaches 25.72 $kJm^{-2}$, increases 50.46% compared with that of the pure PA6 matrix (17.12 $kJm^{-2}$). However, the increase is limited compared with the C-SG/PA6 composites and may be attributed to the poor compatibility and low adhesion between raw-CF and PA6 matrix (as shown in Figure 6b). The impact strength of the C-SG/PA6 composites shows a notable increase along with the content of C-SG. The impact strength of the 13 wt % content C-SG/PA6 composite is 36.52 $kJm^{-2}$ and its impact property increases by 113.17%. The increased compatibility and adhesion between filler and matrix, which aroused by the modified SG with PDDA, is contribute to better toughening effect on the matrix. Figure 9 shows the TGA curves of pure PA6 resin and PA6 composites with the filler content is

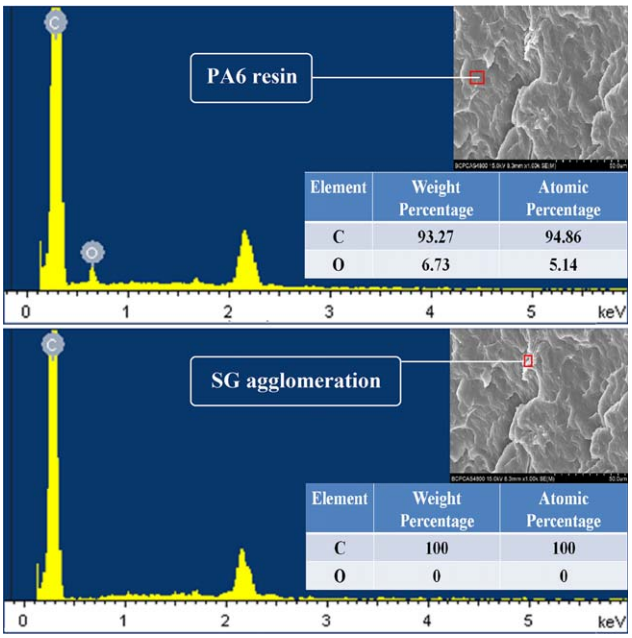


**Figure 7.** Elemental analysis of the SG/PA6 composite in different regions. [Color figure can be viewed in the online issue, which is available at wileyonlinelibrary.com.]

5% under nitrogen. It could be found that the thermo stability of PA6 composites was higher than pure PA6 resin, which aroused by the filler could hinder the rotate of molecular chain of PA6, then the speed the degradation of PA6 was slowed down.

Figure 10 shows the effect of different filler content on the bending properties of PA6 composites. It can be seen that the bending properties exhibits a similar tendency compared to the impact strength along with the content of filler increase. The bending strength and modulus of SG/PA6 composites are decreased with increase in SG content, which may be due to the appearance of SG agglomerates. When the content of raw-CF is

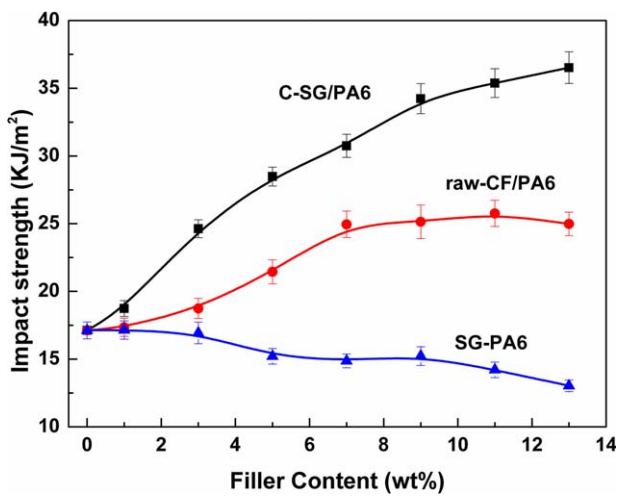


**Figure 8.** Effect of different kinds of filler content on impact strength of PA6 composites. [Color figure can be viewed in the online issue, which is available at wileyonlinelibrary.com.]

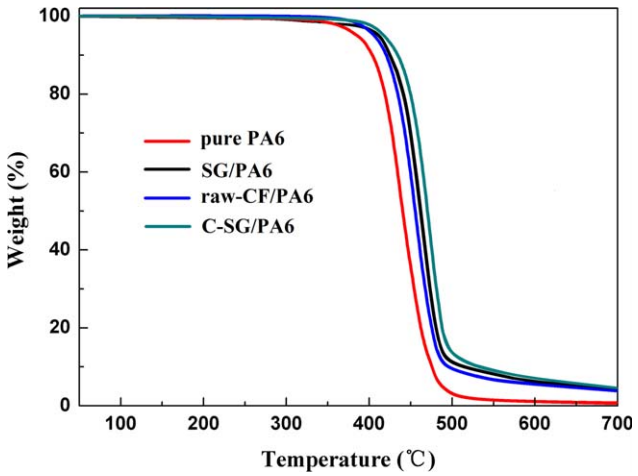


**Figure 9.** TGA curves of pure PA6 and PA6 composites. [Color figure can be viewed in the online issue, which is available at wileyonlinelibrary.com.]

less, the strengthening effect is not obvious. After the raw-CF is continuously filled into the PA6 resin until 11%, the bending strength and modulus be made to rise 34.65% and 34.34% compared to pure PA6 matrix, respectively. Further increase in raw-CF content would not beneficial to bending properties (namely, bending strength, and modulus) of PA6 composites, due to the poor compatibility of the interface between raw-CF and PA6. It can be clearly seen from Figure 8 that the bending properties improvement is best when the C-SG is added into the matrix. Interestingly, with small amount of C-SG content, the strengthening effect is notable. The bending strength and modulus of the 13 wt % content C-SG/PA6 composites are 180.59 MPa and 4927.46 MPa, respectively. Compared with the pure PA6 resin, the two performance indices on bending properties increase by 67.31% and 42.30%, respectively. It can be explained by two factors for the great enhancement of C-SG/PA6 composites: (i) the flexible P-SG with a large surface area on the CF could increase the contact surface area and compatibility between filler and polymer matrix; (ii) the C-SG could form a more effective 3D framework in transmitting loading between the matrix and the fillers. Figure 11 depicts the structure of the C-SG/PA6 composites. The multiscale structure could overcome the shortage of raw-CF, meanwhile, endows the carbon fiber with the special mechanism of reinforcing and toughening. With the modification by PDDA, the P-SG worked as the double-faced adhesive tape, one side linked with the CF and the other side linked with the PA6 matrix, which realizes efficient stress transfer between the PA6 resin and the CF. Consequently, the stiffness and elasticity of C-SG/PA6 composites will be increase.

### Electrical Conductivity

The electrical conductivity of PA6 composites with different kinds of filler were tested by four-probe scheme at room temperature. Electrical conductivity is affected by the fillers structure quality within the matrix, loading, dispersion and the compatibility between the fillers and the polymer matrix. Figure 12 shows the plots of electrical conductivity versus filler content

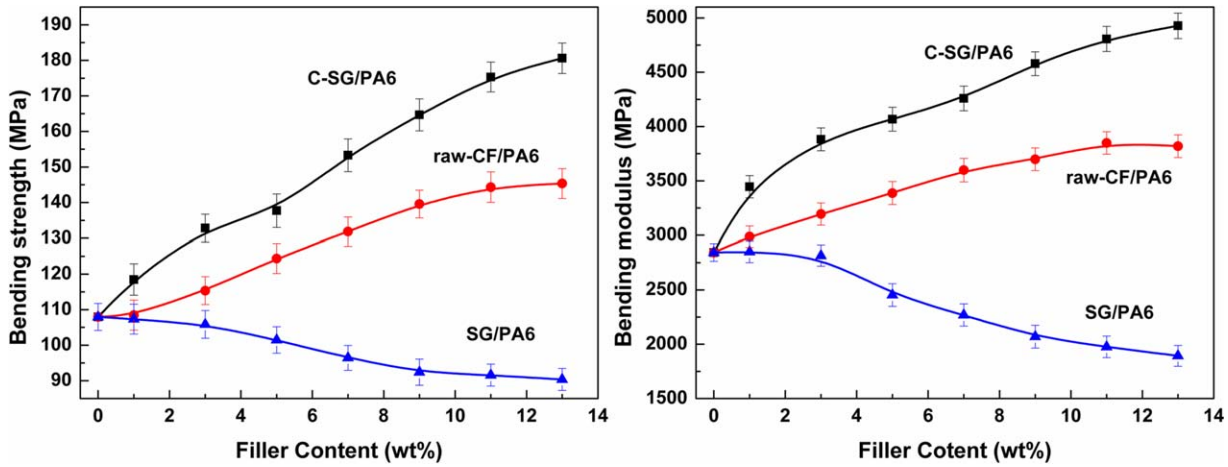


**Figure 10.** Effect of different kinds of filler content on (a) bending strength and (b) bending modulus of PA6 composites. [Color figure can be viewed in the online issue, which is available at wileyonlinelibrary.com.]

for PA6 composites filled with different fillers. It can be seen that the raw-CF/PA6 composites exhibit the poorest electrical conductivity of all composites. The percolation threshold of the raw-CF/PA6 composites is about at the filler content of 5.5 vol %, and the least volume resistivity is about $7.6 \times 10^3$ Ω.cm. By contrast, the SG/PA6 composites reveal a better electrical conductivity, as compared with the PA6 composites containing raw-CF. The percolation threshold of the SG/PA6 composites is about at 1.0 vol %, and the least volume resistivity is about 26 Ω.cm. This is because that the intrinsic electrical conductivity of the SG is much higher than the raw-CF, so it could form an effective conductive network with a small amount of SG. However, the highest electrical conductivity of SG/PA6 composite needs a much higher content of SG, which would increase the cost for practical application for common use. This phenomenon is aroused by the appearance of SG agglomerates in the PA6 matrix, resulting in the reduced effective connection of SG with each other within PA6 matrix. Furthermore, the C-SG/PA6 composites exhibit an interesting curve of electrical conductivity compared to other PA6 composites. The percolation threshold of C-SG/PA6 composites is about at 3.0 vol %, and the least volume resistivity is about 6.0 Ω.cm. It can be seen from Figure 10 the C-SG/PA6 composites possess the highest increase rate of electrical conductivity compared with raw-CF/PA6 and SG/PA6 composites in the percolation area. Meanwhile, the volume resistivity reduction of the C-SG/PA6 composite was greater than that of raw-CF/PA6 and SG/PA6 composite. There are two advantages in the C-SG/PA6 composite: (i) because of the content of SG in C-SG is less than 1 wt %, so the cost of the C-SG is very low compare with the use of individual graphene (SG) within the PA6 composite; (ii) the use of C-SG could endow the PA6 composite with the same electrical conductivity by less filler content and with higher electrical conductivity by the same filler content compared to the addition of raw-CF in PA6 resin. A model was proposed to present the efficient network of raw CF and C-SG for electron transfer in PA6 matrix (as shown in Figure 13). The conductive network composed by the C-SG may be existed some synergetic effect between carbon fiber

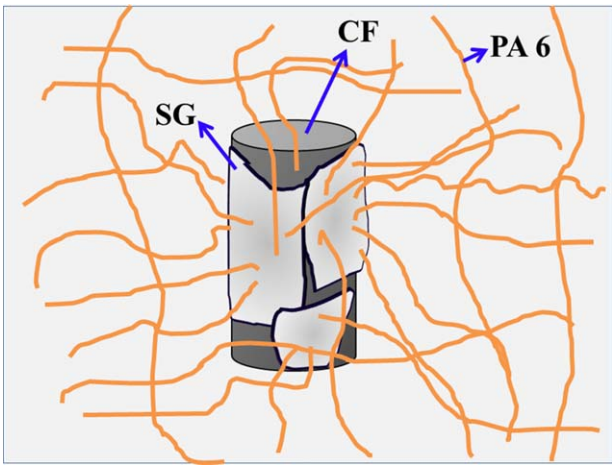


**Figure 11.** Model structure of C-SG/PA6 composites. [Color figure can be viewed in the online issue, which is available at wileyonlinelibrary.com.]

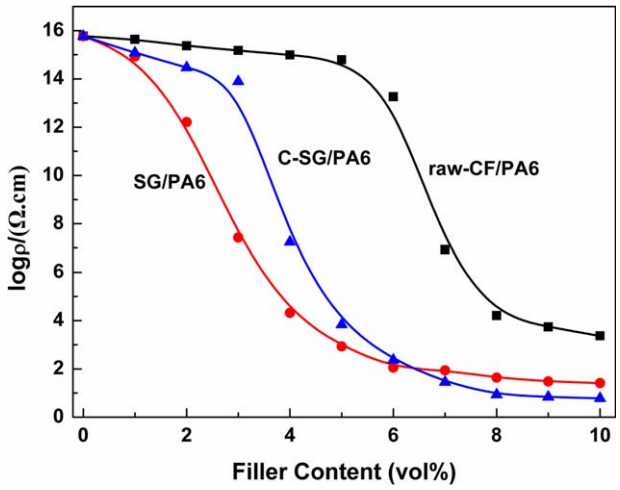


**Figure 12.** Electrical conductivity of raw-CF/PA6, SG/PA6, and C-SG/PA6 composites. [Color figure can be viewed in the online issue, which is available at wileyonlinelibrary.com.]

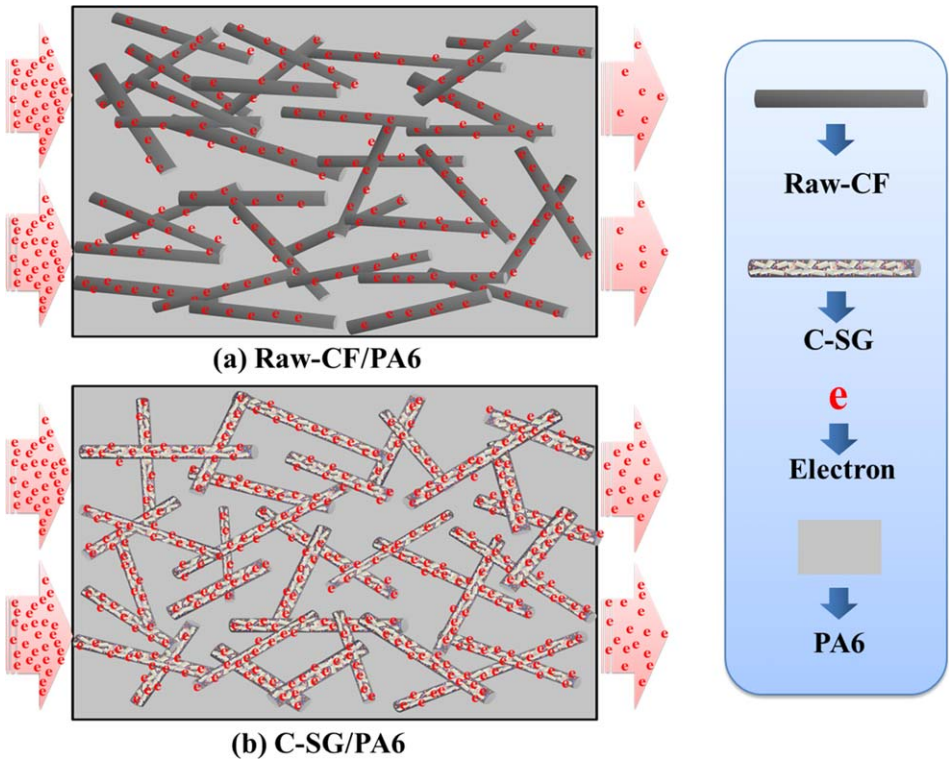


**Figure 13.** The model of electron transfer pattern for (a) raw-CF/PA6 and (b) C-SG/PA6 composites. [Color figure can be viewed in the online issue, which is available at wileyonlinelibrary.com.]

and graphene. Thereby, the transmission of electron in the C-SG/PA6 composite could be realized in three ways: (i) CF-to-CF; (ii) SG-to-SG; (iii) CF-to-SG. These three ways are the main reasons for the observed positive effect of C-SG on the improvement in electrical conductivity of PA6 composites.

## CONCLUSION

In summary, a strategy was designed to improve the mechanical properties and the electrical conductivity of PA6 composites via the combination of SG and CF through the strengthened electrostatic interaction. The impact strength, bending strength and bending modulus of 13 wt % C-SG/PA6 composites were improved by 113.17%, 67.31%, and 42.30%, respectively, compared to pure PA6 resin. The least volume resistivity of the C-SG/PA6 composite is about 6.0 Ω.cm. The PDDA modified SG as the double faced adhesive tape linked CF with PA6 resin, resulting in the improved compatibility of the interface between the fillers and matrix. The mechanical properties and electrical conductivity of C-SG/PA6 composites exhibited the best enhancement compared to CF and SG in PA6 matrix. Since the C-SG is compatible to many polymer systems, we believe that the C-SG could be applied as one of the excellent fillers for many other polymer composites to improve the mechanical and electrical properties.

## ACKNOWLEDGMENTS

This study is supported by the Doctoral Fund of Ministry of Education of China (number: 20121101110014).

## REFERENCES

1. Roy, N.; Sengupta, R.; Bhowmick, A. K. *Prog. Polym. Sci.* **2012**, *37*, 781.
2. Kuilla, T.; Bhadra, S.; Yao, D.; Kim, N. H.; Bose, S.; Lee, J. H. *Prog. Polym. Sci.* **2010**, *35*, 1350.
3. Kiliaris, P.; Papaspyrides, C. D. *Prog. Polym. Sci.* **2010**, *35*, 902.
4. Gong, J.; Niu, R.; Tian, N. N.; Cheng, X. C.; Wen, X.; Liu, J.; Sun, Z. Y.; Mijowska, E.; Tang, T. *Polymer* **2014**, *55*, 2998.
5. Yang, S. Y.; Lin, W. N.; Huang, Y. L.; Tien, H. W.; Wang, J. Y.; Ma, M. C. C.; Li, S. M.; Wang, Y. S. *Carbon* **2011**,*49*, 793.
6. Yang, K.; Gu, M. Y.; Guo, Y. P.; Pan, X. F.; Mu, G. H. *Carbon* **2009**, *47*, 1723.
7. Kilbride, B. E.; Coleman, J. N.; Fraysse, J.; Fournet, P.; Cadek, M.; Drury, A.; Hutzler, S.; Roth, S.; Blau, W. J. *J. Appl. Phys.* **2002**, *92*, 4024.
8. Berber, S.; Kwon, Y. K.; Tomanek, D. *Phys. Rev. Lett.* **2000**, *84*, 4616.
9. Lonjon, A.; Demot, P.; Dantras, E.; Lacabanne, C. J. *J. Non-Cryst. Solids.* **2012**, *358*, 1859.
10. Argon, A. S.; Cohen, R. E. *Polymer* **2003**, *44*, 6013.
11. Florian, P.; Christian, H. *Polymer* **2014**, *55*, 3015.
12. Zhang, H. B.; Zheng, W. G.; Yan, Q.; Yang, Y.; Wang, J. W.; Lu, Z. H.; Ji, G. Y.; Yu, Z. Z. *Polymer* **2010**, *51*, 1191.
13. Lin, C.; Chung, D. D. L. *Carbon* **2009**, *47*, 295.
14. Zhao, X.; Zhang, H. Q.; Chen, D. J.; Lu, P. *Macromolecules* **2010**, *43*, 2357.

15. Stankovich, S.; Dikin, D. A.; Dommett, G. H. B.; Kohlaas, K. M.; Zimney, E. J.; Stach, E. A. *Nature* **2006**, *442*, 282.
16. Zhang, B.; Asmatulu, R.; Soltani, S. A.; Le, L. N.; Kumar, S. S. A. *J. Appl. Polym. Sci.* **2014**, *131*, doi: 10.1002/app.40826.
17. Zhang, Y. B.; Tan, Y. W.; Stormer, H. L.; Kim, P. *Nature* **2005**, *438*, 201.
18. Ramanathan, T.; Abdala, A. A.; Stankovich, S.; Dikin, D. A.; Herrera-Alonso, M.; Piner, R. D. *Nat. Nanotechnol.* **2008**, *3*, 327.
19. Si, Y.; Samulski, E. T. *Chme. Mater.* **2008**, *20*, 6792.
20. Si, Y.; Samulski, E. T. *Nano. Lett.* **2008**, *8*, 1679.
21. Li, D.; Muller, M. B.; Gilje, S.; Kaner, R. B.; Wallace, G. G. *Nat. Nanotechnol.* **2008**, *3*, 101.
22. Yang, S. Y.; Ma, C. C. M.; Teng, C. C.; Huang, Y. W.; Liao, S. H.; Huang, Y. L.; Tien, H. W.; Lee, T. M.; Chiou, K. C. *Carbon* **2010**, *48*, 592.
23. Datsyuk, V.; Kalyva, M.; Papagelis, K.; Parthenios, J.; Tasis, D.; Siokou, A.; Kallitsis, I.; Galiotis, C. *Carbon* **2008**, *46*, 833.
24. Zhang, X. Q.; Fan, X. Y.; Yan, C.; Li, H. Z.; Zhu, Y. D.; Li, X. T.; Yu, L. P. *Appl. Mater. Inter.* **2012**, *4*, 1543.
25. Ning, N. Y.; Zhang, W.; Yan, J. J.; Xu, F.; Wang, T. N.; Su, H.; Tang, C. Y.; Fu, Q. *Polymer* **2013**, *54*, 303.
26. Eswaraiah, V.; Sasikaladevi, S. H.; Aravind, J. M.; Ramaprabhu, S. *J. Mater. Chem.* **2011**, *21*, 6800.
27. Stankovich, S.; Piner, R. D.; Nguyen, S. T. *Carbon* **2006**, *44*, 3342.
28. Stankovich, S.; Piner, R. D.; Chen, X. Q.; Wu, N. Q.; Nguyen, S. T. *J. Mater. Chem.* **2006**, *16*, 155.
29. Wang, S. J.; Jiang, S. P.; Wang, X. *Nanotechnology* **2008**, *19*, 265601.
30. Vianyan, B. P.; Nargar, R.; Sethupathi, K.; Ramaprabhu, S. *J. Phys. Chem. C* **2011**, *115*, 15679.
31. Omar, G. V.; Raquel, L. R.; Enrique, S. G.; Luis, Y.; Sergio, M.; Ronald, F. *Polymer* **2014**, *55*, 2347.
32. Li, K. P.; Zhang, J. J.; Yang, G. H.; Wang, C. M.; Zhang, J. J. *Electrochem. Commun.* **2010**, *12*, 402.
33. Wang, S. Y.; Yu, D. S.; Dai, L. M.; Chang, D. W.; Baek, J. B. *ACS Nano* **2011**, *5*, 6202.
34. Dong, J.; Yin, C. Q.; Zhao, X.; Li, Y. Z.; Zhang, Q. H. *Polymer* **2013**, *54*, 6415.
35. Wang, S. Y.; Jiang, S. P.; Wang, X. *Nanotechnology* **2008**, *19*, 265601.
36. Sumanta, S.; Pallab, B.; Goutam, H.; Debasis, G.; Chapal, K. D. *J. Appl. Polym. Sci.* **2013**, *128*, 1476.